L-Band Radar Estimation of Forest Attenuation for Active/Passive Soil Moisture Inversion

Mehmet Kurum, Roger H. Lang, *Fellow, IEEE*, Peggy E. O'Neill, *Senior Member, IEEE*, Alicia T. Joseph, Thomas J. Jackson, *Fellow, IEEE*, and Michael H. Cosh

Abstract—In the radiometric sensing of soil moisture through a forest canopy, knowledge of canopy attenuation is required. Active sensors have the potential of providing this information since the backscatter signals are more sensitive to forest structure. In this paper, a new radar technique is presented for estimating canopy attenuation. The technique employs details found in a transient solution where the canopy (volume-scattering) and the tree–ground (double-interaction) effects appear at different times in the return signal. The influence that these effects have on the expected time-domain response of a forest stand is characterized through numerical simulations. A coherent forest scattering model, based on a Monte Carlo simulation, is developed to calculate the transient response from distributed scatterers over a rough surface. The forest transient-response model for linear copolarized cases is validated with the microwave deciduous tree data acquired by the Combined Radar/Radiometer (ComRAD) system. The attenuation algorithm is applicable when the forest height is sufficient to separate the components of the radar backscatter transient response. The frequency correlation functions of double-interaction and volume-scattering returns are normalized after being separated in the time domain. This ratio simply provides a physically based system of equations with reduced parameterizations for the forest canopy. Finally, the technique is used with ComRAD L-band stepped-frequency data to evaluate its performance under various physical conditions.

Index Terms—Attenuation, frequency correlation function (FCF), microwave transient response, soil moisture, vegetation.

I. INTRODUCTION

SOIL moisture is a basic parameter that integrates much of the land-surface hydrology and provides a basic link between the Earth's surface and the atmosphere through its effect on surface energy and moisture fluxes. Soil moisture is thus a key variable in the hydrologic cycle. To understand the role of land-surface hydrology in regional and global processes, the distribution of soil moisture under a variety of surface conditions must be mapped accurately. Microwave remote sensing offers great potential for accurate soil moisture estimation on a global basis because the primary physical property that affects the microwave measurement is directly dependent on the amount of water present in the soil. This potential, coupled with advances in microwave sensor technology, has given rise to new satellite missions with L-band passive microwave radiometers. The European Space Agency Soil Moisture and Ocean Salinity (SMOS) mission (scheduled to launch in 2009), for example, will use an L-band 2-D interferometric radiometer design providing about 50-km resolution [1]. The U.S. National Research Council Committee on Earth Science and Applications from Space has recently recommended the Soil Moisture Active and Passive (SMAP) mission, which is expected to launch around 2013 [2]. SMAP will use a combined L-band radiometer and high-resolution radar to produce a global 10-km surface soil moisture data product. It is expected that these missions will significantly increase the capability of monitoring the Earth's soil moisture globally.

Although L-band radiometry is preferable for soil moisture sensing due to its great sensitivity to the moisture content of the first 5 cm of soil, the pixel size expected from L-band spaceborne radiometers is on the order of several tens of kilometers. As a result, one expects that the surface within a large radiometric footprint will be a mixture of different surface and vegetation types. Forests, for example, will fill many pixels partially or completely in the future spaceborne radiometric images of emitted microwave radiation since forests cover a considerable portion of the Earth's land surface. An important question is whether, in light of this coarse limit on resolution, the spaceborne instruments can make meaningful measurements of average soil moisture over a landscape that is partially or completely covered with a forest canopy.

Forest canopies attenuate the emission from ground and reduce the radiometric sensitivity to soil moisture [3], [4]. To correct for this reduced emission, one must measure the canopy attenuation which depends on canopy architecture and foliage water content. The preferred method for determining the biophysical properties of tree canopies is active remote sensing since active sensors provide very high spatial resolution data and yield better information about the canopy architecture [5], [6]. To assess the accuracy and reliability of the soil moisture products derived over forested regions, SMOS and SMAP are likely to benefit from the current and future

L-band radar sensors such as the Advanced Land Observing Satellite-Phased Array L-band SAR [7] and the Deformation, Ecosystem Structure and Dynamics of Ice (DESDynI) (L-band InSAR and Multibeam Lidar) [2]. These new-generation radar sensors would have the potential of providing the complementary information needed in radiometric soil moisture algorithms in forested terrains since the backscatter signals at L-band are more sensitive to forest biophysical properties. In fact, the integrated active/passive microwave sensor approach to measure soil moisture is recognized as the future direction for the global mapping of soil moisture [2]. This paper presents one such study which is using a ground-based active/passive L-band instrument system named Combined Radar/Radiometer (ComRAD). The objective of this paper is to develop a new radar attenuation algorithm for better interpretation of radiometric measurements acquired over small stands of deciduous trees by ComRAD and to provide an insight into the problem of scattering from forests in the time domain.

A number of different radar approaches aimed at characterizing the propagation in tree canopies have been reported in the past [8]–[10]. Traditionally, a large number of independent radar observations (frequency, polarization, and spatial diversity) in conjunction with some *a priori* information about the forest stand have been used for estimating the biophysical parameters of the forest stands. The use of polarimetric SAR data at L- and C-bands to estimate basal area, height, and dry crown biomass for forested areas is one example [8]. A semiempirical algorithm for deriving the spatial distributions of water content and biomass over local and regional scales from polarimetric SAR measurements at P- and L-band channels was used in [9]. In [10], forest height, average forest extinction, and the underlying topography were estimated using the interferometric coherence and phase information in different polarizations. However, the common problem in all estimation techniques arises from the fact that the predicted backscatter properties depend on a large number of input parameters that makes the inversion process difficult.

One solution to this problem can be the identification of different backscattering sources within the forest canopy in the transient response of the backscattered field. In modeling a forest canopy, two dominant scattering mechanisms are taken into account: the volume-scattering and the double-interaction contributions. The relative contribution of each mechanism in the total backscatter signal of the imaging radar can vary depending on the structural characteristics of the forest canopy and the moisture content of the underlying soil [11]. A time-domain analysis can be used as a tool to distinguish the characteristics of the forested terrain as a function of depth by utilizing different arrival times of the components of the transient response. Theoretical studies of the transient response of a random medium over ground were made by Le Vine *et al.* [12] and Kilic and Lang [13]. It has been shown that each contribution can be used as a means for obtaining additional information about the layer. A significant ground return in the backscatter pulse signature that provides soil moisture information was reported in [14]. Using a helicopter-borne ranging radar, Hyyppa and Hallikainen [15] observed significant changes in the forest canopy profile for different stand types. Martinez *et al.* [16]

Fig. 1. ComRAD microwave instrument system deployed over a stand of Paulownia trees.

used high vertical resolution backscatter profiles to validate a radiative transfer model coupled with the tree architecture.

In this paper, a new technique to determine canopy attenuation from stepped-frequency measurements over trees is proposed. The algorithm for the estimation of canopy attenuation is based on separating the canopy and tree–ground returns. Once these backscattering sources are identified in the time domain and are isolated with a gating filter, the frequency correlation functions (FCFs) for each backscattering contribution are generated. The ratio of canopy to trunk–ground return is computed to eliminate system characteristics such as antenna gain. The ratios are calculated for an array of frequency spacings over the system bandpass. The resulting system of equations only depends on the canopy thickness, the canopy attenuation, and a combined parameter involving the forest scattering coefficients and the ground reflectance. A least square method is used to solve for the attenuation and the combined parameter assuming that the canopy thickness is estimated *a priori* from the transient response. In order to understand the sensitivity of the technique to various physical conditions and incidence angles, a ComRAD active/passive microwave truck instrument system was used. ComRAD was jointly developed and operated by the National Aeronautics and Space Administration (NASA) Goddard Space Flight Center and The George Washington University. As shown in Fig. 1, data collected by the ComRAD system were acquired over deciduous Paulownia trees under *leaf-drop* and *full-canopy* conditions at incidence angles of 15°, 25°, 35°, and 45°.

The outline of this paper is as follows. In Section II-A, a coherent scattering model in conjunction with a Monte Carlo simulation is used to obtain the transient response from a

layer of randomly distributed scatterers. Section II-B introduces the ComRAD microwave instrument system. The description of the site and the experiment are summarized in detail in Section II-C. In Section II-D, time-domain simulations using these data are carried out for various cases in order to understand backscattering sources within a forest canopy and their effects on the transient response of the backscattered field. The average simulated and measured backscatter transient responses of Paulownia trees under *full-canopy* and *leaf-drop* conditions at $45°$ for horizontal (HH) and VV polarizations are compared. In Section III, a new technique for determining the canopy attenuation using the measured stepped-frequency radar backscatter response is described in detail. The extracted attenuation values from both simulated and measured data at the ComRAD angles are presented and discussed at the end of this section.
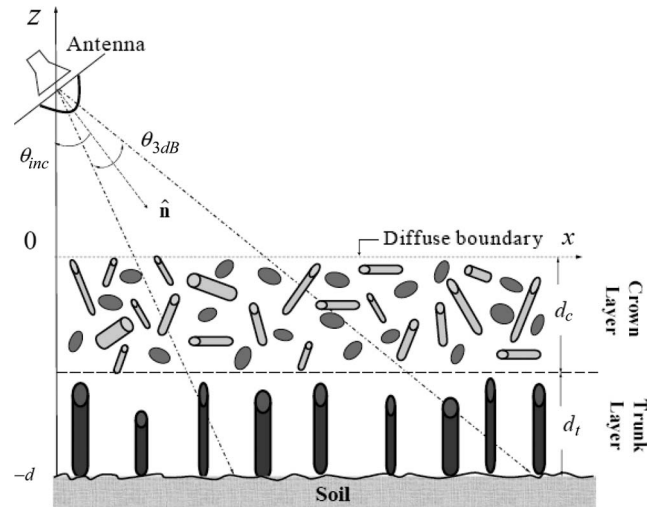

Fig. 2. Discrete random medium consisting of two layers of vegetation over a rough ground surface. The thicknesses of the crown and trunk layers are represented by d_c and d_t, respectively.

II. TIME-DOMAIN ANALYSIS OF RADAR BACKSCATTER RESPONSE

In this section, a coherent scattering model in conjunction with a Monte Carlo simulation is developed to calculate the time-domain response from a forested terrain. In the scattering model, individual tree components are randomly embedded in a mean medium using their statistical characteristics, and then, the scatterers are illuminated by an antenna. The model assumes no knowledge of the incident field on the random medium and therefore holds for any arbitrary waveform. Using the distorted Born approximation (DBA), the total backscattered field in the frequency domain is obtained from the coherent sum of the scattered field from each scatterer. DBA is a first-order scattering approximation where the incident wave travels through the mean medium (equivalent medium) and is scattered by the particles embedded in this medium. The attenuation and phase change of the coherent wave, propagating in the equivalent medium, is found by calculating the mean field within the medium. A similar approach for calculating the backscattered electric field was carried out by Lang *et al.* [17].

The coherent scattering model developed in this paper preserves the phase of the backscattered field from the forest canopy. Having the phase and amplitude information allows us to calculate the time-domain response using frequency-domain solutions, which are calculated at discrete frequency points in the operating bandwidth of the radar. The transient response is produced by performing an inverse discrete Fourier transform (IDFT) on this backscattered field. This follows closely the data acquisition and signal processing technique employed by network-analyzer-based radars (stepped-frequency measurements). An average time-domain response is obtained by a sufficient number of realizations of trees through Monte Carlo simulations. From an intuitive and data-analysis point of view, it is desirable to have time-domain information. With the time-domain information, one acquires the ability to locate spatially the individual backscattering sources within the forest canopy. For example, the volume-scattering and double-interaction contributions appear at different times in the transient solution. This time difference results from the fact that these two scattering mechanisms have different path lengths. To illustrate this point

and to characterize the time-domain scattering mechanisms of a backscatter radar response under various physical conditions, several plots will be presented at the end of this section.

A. Forest Transient-Response Model

An aperture antenna with an arbitrary but known radiation pattern is considered to be overlooking a forest canopy. The forested terrain consists of two layers of vegetation over a dielectric half-space with an underlying rough surface to characterize the ground as shown in Fig. 2. The two-layer model is often used for trees where a clear boundary between the crown and trunk layers can be identified. It is assumed that the crown layer consists of randomly distributed branches and leaves, and the trunk layer consists of vertically distributed tree trunks. The branches and trunks are modeled as finite dielectric cylinders, and the leaves are modeled as thin dielectric disks. The backscatter configuration considered here assumes that the regular far-field conditions are met. In order for the regular far-field conditions to hold, the following must be true: 1) Each scatterer in the vegetation layer is in the far zone of the antenna, and 2) the antenna is in the far zone of each scatterer within the layer.

It will also be assumed that the transmitted signal is a narrowband signal, i.e., the pulse is confined to a bandwidth B, centered on a nominal carrier frequency f_c, where $B/f_c \ll 1$. In practical situations, the narrowband assumption is quite reasonable and often can be used to model very narrow pulses. The minimum range resolution available is determined by the modulating bandwidth B of the radar and is given by $c/2B$ in radial direction, where c is the speed of light. In the case of the remote sensing of vegetation at L-band such as 1.25 GHz, a 100-MHz bandwidth would result in a pulse with the range resolution of 1.5 m long. The pulse is comparable or longer than the thickness of a typical agricultural vegetation canopy, but it is sufficiently short to probe tall forest stands.

The transmitted fields from the antenna are decomposed into their plane-wave components by a Fourier transform. Then,

by utilizing the assumption (1) aforementioned, each spectral component by means of a stationary phase evaluation is asymptotically related to the angular distribution of transmitted radiation traveling in different directions [18]. Then, the solution to an illumination of a discrete random medium over ground by a plane wave [19], [20] is applied to each transmitted ray to find the scattered fields from the discrete scatterers embedded in the mean medium. In [18], the radar is directly incorporated into the analytical wave theory in conjunction with DBA. The source of each ray of the spatial spectrum of the scattered field at the antenna is associated with the statistical characteristics of individual scatterers in the mean media by means of DBA. Finally, the backscattered signal received by the radar is expressed as a weighted coherent sum involving the antenna spatial spectrum and backscattered radiation [21]. This analytical wave formulation accounts for the spread of the beam within the medium and for the variation of the attenuation and the phase with the propagation direction.

The propagation constant of the coherent wave through the canopy layer can be calculated by employing Foldy's theory for the mean wave propagation in a discrete random medium. Under the assumption that the scatterers are uniformly distributed in azimuth, the following expression for the propagation constant $\kappa_{eq}(\hat{\mathbf{i}})$ is obtained in terms of the forward scattering amplitudes of individual components:

$$\kappa_{eq}(\hat{\mathbf{i}}) = k_0 \cos\theta_i + \Delta\kappa_{eq}(\hat{\mathbf{i}})$$

$$\Delta\kappa_{eq}(\hat{\mathbf{i}}) = \frac{2\pi}{k_0 \cos\theta_i} \sum_\alpha \rho_\alpha \overline{f_{qq}^{(\alpha)}}(\hat{\mathbf{i}}, \hat{\mathbf{i}}) \tag{1}$$

where $\hat{\mathbf{i}}$ is a unit vector in the direction of propagation, k_0 is the free-space wavenumber, and θ_i is the angle between the unit vector $\hat{\mathbf{i}}$ and z-axis. The summation index $\alpha \in \{L, B, T\}$ denotes the scatterer types such as leaves (L), branches (B), and trunks (T). The number density of the scatter type α is given by ρ_α. Here, the quantity $f_{pq}^{(\alpha)}(\hat{\mathbf{o}}, \hat{\mathbf{i}})$ denotes the bistatic scattering amplitude of the scatter type α, where $\hat{\mathbf{i}}$ is in the direction of the incident wave and $\hat{\mathbf{o}}$ is in the direction of the observation point. Unit vectors are represented as a bold symbol with a hat over them. The bar over the scattering amplitude denotes ensemble average over the angular and size statistics of particles.

Under the assumption of single scattering, the received backscattered field due to an individual particle of type α embedded in the mean medium over a ground plane is composed of three types of contributions: a direct (volume-scattering) term (d), direct-reflected (double-interaction) terms $(dr1$ and $dr2)$, and a reflected term (r), as shown in Fig. 3. The received backscatter electric field from this particle can be expressed as the coherent sum of these individual contributions, which is given by

$$E_{pq}^{(\alpha)}(f) = E_{pqd}^{(\alpha)}(f) + E_{pqdr1}^{(\alpha)}(f) + E_{pqdr2}^{(\alpha)}(f) + E_{pqr}^{(\alpha)}(f) \tag{2}$$

where p and q denote the transmit and receive polarizations, respectively. The quantities p and q can be horizontal (H) or vertical (V), and as a result, co- and cross-polarized cases are treated simultaneously. The subscripts in (2) refer to the scattering-mechanism types. For the sake of simplicity, a one-layer model for the development of the analytical formulations will be considered here. However, the simulations will be run for the two-layer model since it is more realistic for the trees being considered. Note that a time variation of $\exp(-i\omega t)$ is assumed and suppressed in this paper.

The contributions given in (2) are as follows.

1) *Direct Contribution*: This contribution is composed of waves that scatter directly back to the receiving antenna. The configuration is shown in Fig. 3(a), where an antenna located at the point A illuminates a scatterer of type α positioned at the point $S = (x_\alpha, y_\alpha, -z_\alpha)$ in the equivalent medium. The strength of the incident mean field on this particle is directly proportional to the value of the antenna radiation pattern along the $\hat{\mathbf{r}}_1$ direction where the unit vector $\hat{\mathbf{r}}_1$ is defined in the direction from the point A to S. The received backscattered wave for the direct contribution is given by

$$E_{pqd}^{(\alpha)}(f) = K \frac{e^{i2k_0 r_1}}{r_1^2} G_{pq}(-\hat{\mathbf{r}}_1, \hat{\mathbf{r}}_1) f_{pq}^{(\alpha)}(-\hat{\mathbf{r}}_1, \hat{\mathbf{r}}_1)$$

$$\times \left[e^{i\Delta\kappa_{ep}(-\hat{\mathbf{r}}_1)z_\alpha} e^{i\Delta\kappa_{eq}(\hat{\mathbf{r}}_1)z_\alpha} \right] \tag{3}$$

where $K = -ia^*/2k_0$ is constant, a is the incident wave at the antenna port in transmission, a^* denotes the complex conjugate of a, and r_1 is equal to AS, which is the distance between points A and S. The antenna gain function $G_{pq}(\hat{\mathbf{o}}, \hat{\mathbf{i}})$ is defined by

$$G_{pq}(\hat{\mathbf{o}}, \hat{\mathbf{i}}) = \frac{4\pi F_p(\hat{\mathbf{o}}) F_q(\hat{\mathbf{i}})}{|a|^2} \tag{4}$$

where $|a|^2$ is the available power, $\hat{\mathbf{i}}$ denotes the direction of a q-polarized radiated wave, $\hat{\mathbf{o}}$ denotes the direction of a p-polarized received wave, and the antenna farfield q-polarized radiation pattern is given by $F_q(\hat{\mathbf{i}})$. The radiation pattern is chosen proportional to the radiated electric field such that the square of its norm integrated over a unit sphere equals the average radiated power [21]. A generalized Gaussian antenna pattern, including sidelobes, is assumed as an approximation to the radiation pattern needed in this formulation. This pattern will be assumed to be circularly symmetrical about the direction of peak intensity.

2) *Direct-Reflected Contribution:* This contribution is composed of two types of backscattered waves. A backscattered wave of the first type consists of an incident wave that is bistatically scattered from the particle located at point S and then specularly reflected from point G back to the receiver. The point G is the specular point at the lower interface. The mechanism of type 1 is shown in Fig. 3(b). Backscattered waves of the second type have exactly the opposite trajectory. It should be noted that both type 1 and type 2 rays have exactly the same length of ray trajectory.
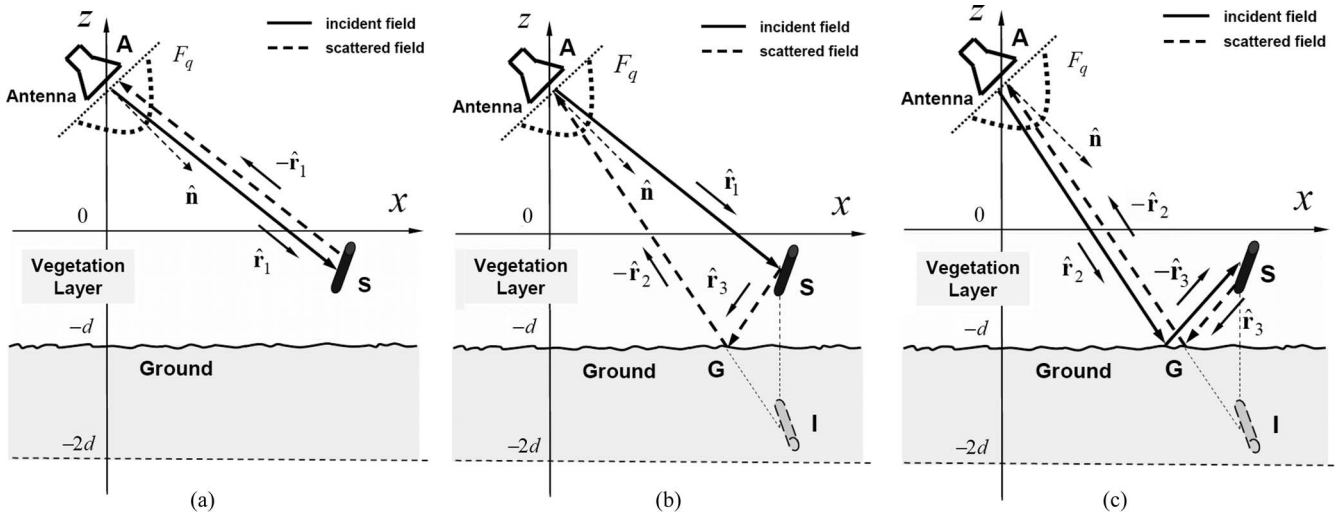
Fig. 3. Scattering mechanisms of the field for the backscatter case: (a) shows the *direct* term. (b) shows the *direct-reflected* term type 1. (c) shows the *reflected* term.

As a result, the rays interfere coherently and cause an enhancement effect. The received backscattered fields, due to type 1 and type 2 direct-reflected contributions, are given, respectively, by

$$E_{pqdr1}^{(\alpha)}(f) = K \frac{e^{ik_0 r_2} e^{ik_0 r_1}}{r_2 r_1} G_{pq}(-\hat{\mathbf{r}}_2, \hat{\mathbf{r}}_1) f_{pq}^{(\alpha)}(\hat{\mathbf{r}}_3, \hat{\mathbf{r}}_1) \Gamma_{gp}$$

$$\times \left[e^{-i\Delta\kappa_{ep}(-\hat{\mathbf{r}}_2)(-2d+z_\alpha)} e^{i\Delta\kappa_{eq}(\hat{\mathbf{r}}_1)z_\alpha} \right] \quad (5)$$

$$E_{pqdr2}^{(\alpha)}(f) = K \frac{e^{ik_0 r_1} e^{ik_0 r_2}}{r_1 r_2} G_{pq}(-\hat{\mathbf{r}}_1, \hat{\mathbf{r}}_2) f_{pq}^{(\alpha)}(-\hat{\mathbf{r}}_1, -\hat{\mathbf{r}}_3) \Gamma_{gq}$$

$$\times \left[e^{i\Delta\kappa_{ep}(-\hat{\mathbf{r}}_1)z_\alpha} e^{-i\Delta\kappa_{eq}(\hat{\mathbf{r}}_2)(-2d+z_\alpha)} \right] \quad (6)$$

where the unit vector $\hat{\mathbf{r}}_2$ is defined in the direction from the antenna at point A to the image of the particle located at point I. r_2 is equal to AI, which is the distance between points A and I. In other words, the distance r_2 represents the total path traveled by the scattered field from the particle to the antenna. One can easily show that $AI = AG + GS$ since $GS = GI$ due to the symmetry. The unit vector $\hat{\mathbf{r}}_3$ is defined in the direction from the scatterer (point S) to the specular point on the ground (point G). The volume–surface interaction terms in (5) and (6) involve Γ_{gq} which is the reflection coefficient of the rough surface. It is assumed that the rough surface under the forest follows Kirchhoff's approximation and has the Gaussian height distribution [22]; therefore, the reflection coefficient of the rough surface is expressed as

$$\Gamma_{gq} = R_{gq} e^{-2(k_0 s \cos\theta)^2} \quad (7)$$

where R_{gq} is the q-polarized Fresnel reflection coefficient of the average dielectric surface, s is the surface rms height, and θ is the angle between the vector $\hat{\mathbf{r}}_3$ (or $\hat{\mathbf{r}}_2$) and the z-axis.

3) *Reflected Contribution:* This contribution is composed of waves that propagate through the medium; they are reflected from the lower interface and then backscattered from a particle and reflected from the lower interface back to the receiver. A diagram of this process is shown in Fig. 3(c). The received backscattered field for the reflected contribution is given by

$$E_{pqr}^{(\alpha)}(f) = K \frac{e^{i2k_0 r_2}}{r_2^2} G_{pq}(-\hat{\mathbf{r}}_2, \hat{\mathbf{r}}_2) f_{pq}^{(\alpha)}(\hat{\mathbf{r}}_3, -\hat{\mathbf{r}}_3) \Gamma_{gp} \Gamma_{gq}$$

$$\times \left[e^{-i\Delta\kappa_{ep}(-\hat{\mathbf{r}}_2)(-2d+z_\alpha)} e^{-i\Delta\kappa_{eq}(\hat{\mathbf{r}}_2)(-2d+z_\alpha)} \right]. \quad (8)$$

In this present investigation, a Monte Carlo procedure is chosen to predict the effects of vegetation and ground parameters on the transient response from a forest canopy. Monte Carlo simulations are very useful to incorporate coherent addition and wave interaction effects in a vegetation canopy. As a result, a more realistic modeling of the forest structure through Monte Carlo simulations can be achieved. The frequency-domain results given previously will be used in Monte Carlo simulations to calculate the time-domain radar backscatter response. Here, a brief description of the Monte Carlo procedure for a two-layer forest canopy is given as follows.

1) The numbers of the scatterers of each type (leaf, branch, and trunk) and of each kind of any type are calculated for the illuminated volume of the trunk and the crown layers. The illuminated volumes are defined by the antenna cross section beamwidth and the crown and trunk layers (see Fig. 2).

2) Each scatterer is embedded in the equivalent medium where a random position is generated for each scatter in the illuminated volume based on whether it belongs to either the crown or the trunk layers; each scatterer is then oriented according to some prescribed orientation statistics.

3) The frequency-domain solutions of the backscattered electric fields $E_{pq}^{(\alpha)}(f)$ over N_f frequency points, spanning the bandwidth, are computed for each particle; these frequency-domain solutions are then summed coherently.
4) The total backscattered field is windowed in the frequency domain before transforming to the time domain. The use of windowing is critical to the generation of usable time-domain data. If the frequency data do not gently decay to zero at each end of its bandpass, the generated time-domain data will be distorted. Windows are applied to the frequency data to force the ends to decay smoothly to zero. The window function used here is the Kaiser–Bessel window with $\beta = 6$ where β controls the amount of roll-off for the window function [23].
5) An IDFT on the total backscattered field is performed to produce the time-domain response $e_{pq}(t)$. Both the frequency- and time-shift theorems have been used to allow any arbitrary frequency range to be transformed into any arbitrary time range [24].
6) Finally, by repeating steps 1)–5) for many realizations of the random medium, the average transient response of the backscattered field is obtained from the time-domain responses averaged over all realizations.

Before going on to show some simulation results, we will describe the experiment along with the site information and introduce the microwave instrument system used during the experiment.

B. Truck-Based Microwave Instrument System

As a part of this multisensor soil moisture research, a coordinated sequence of field measurements involving the ComRAD active/passive microwave truck instrument system was undertaken. Jointly developed and operated by the NASA Goddard Space Flight Center and the George Washington University, ComRAD consists of dual-polarized 1.4-GHz total power radiometers (LH, LV) and a quad-polarized 1.25-GHz L-band radar sharing a single parabolic dish antenna with a novel broadband stacked-patch dual-polarized feed [25]. The instruments are deployed on a truck with a hydraulic boom; they share common control software, real-time calibrated signals, and the capability for automated data collection for unattended operation. A picture of the truck system taking measurements over Paulownia trees is shown in Fig. 1.

The truck radar system is configured around an Agilent E5071B ENA series vector network analyzer that is mounted on the instrument platform at the end of the boom. It operates in a stepped-frequency mode, and therefore, it measures the magnitude and phase of the scattered electric field over N_f frequency points spanning the operating bandwidth for all linear polarization combinations. The operation bandwidth of the radar is 100 MHz, and the gain of the radiation pattern with 12° beamwidth is 19.5 dB. The radar has a capability of computing the IDFT of the measured frequency-domain data to give the time-domain response in real time. Switching between polarizations is accomplished by an HP3488A switching unit outfitted with single-pole double-throw coaxial switches. Signals are routed to and from the antenna elements by the switching unit

TABLE I
EXPERIMENT SITE INFORMATION

Location	Upper Marlboro, Maryland USA
General Ground Surface Conditions	Flat with relatively short grass under the tree canopy.
Soil Texture	Loamy sand, consisting of 80% sand and 7% clay.
Volumetric Soil Moisture (VSM)	24.3% on October 22nd and 32.0% on November 24th
Tree Height	Variable on the order of 11 m - 14 m
Diameters at Breast Height (DBH)	17 cm to 23 cm
Basal Area	25.8 m^2/ha
Biomass	∼13 kg/m^2
Platform Height	19 m

and directional couplers, with bandpass filters installed in the return or received signal path to keep the noise floor on the band as low as possible. An HP8449B preamplifier is used for the amplification of the reflected power from the distributed targets. A remote computer control of the switches, located in the switching unit and the network analyzer, is achieved via Ethernet cables through which all data and control sequences travel.

C. Experiment and Site Description

During Fall 2006 (initial field checkout) and Spring–Fall 2007, ComRAD was deployed to a tree test site at an experimental farm run by the University of Maryland's Central Maryland Research and Education Center [26]. The site consisted of planted stands of deciduous Paulownia trees, a fast-growing deciduous tree with broad leaves. This paper will concentrate on the radar results from a plot whose characteristics are given in Table I. The radar data were collected over the trees under full-canopy (October 22) and leaf-drop (November 24) conditions in 2007. The tree plot has 92 trees in a 1089-m² area. Under full-canopy conditions, the biomass was ∼13 kg/m². Two overflights of the test site were conducted with a portable airborne laser system to acquire spatial information on tree heights and canopy structure [27]. The trees have a clear boundary between the crown and trunk layers where the average thickness of crown and trunk layers are estimated as 6 and 7 m, respectively. The diameter at breast height (DBH) ranges from 17 to 23 cm (average $DBH = 19.4$ cm). The tree heights are variable, on the order of 11–14 m. Radar data were acquired at the height of 19 m over the ground level with incidence angles of 15°, 25°, 35°, and 45°. The corresponding footprints on the ground at these angles were 16.5, 20.1, 27.4, and 43.2 m², respectively. During the radar measurements, the truck boom was rotated in a conical scan arrangement with a 60° sweep in azimuth.

TABLE II
CANOPY PARAMETERS FROM MEASUREMENTS

Tree Components	Av. Length (cm)	Av. Radius (cm)	Density (m^{-3})	Orientation
Trunks	617.0	8.73	0.0055	Vertical
Primary br.	171.0	4.80	0.0055	Uni. $20 - 50^0$
	245.0	4.22	0.0055	Uni. $20 - 50^0$
	120.0	3.84	0.0055	Uni. $20 - 50^0$
Secondary br.	153.8	1.58	0.1877	Uni. $10 - 60^0$
	63.6	0.98	0.7344	Uni. $0 - 90^0$
	48.1	0.45	1.9326	Uni. $0 - 90^0$

	Av. Thickness (mm)	Av. Radius (cm)	Density (m^{-3})	Orientation
Leaves	0.12	10.2	11.121	Uni. $0 - 90^0$

Measurements were made at 28 locations, approximately one every $2°$.

Although the soil texture at the site was a loamy sand, consisting of 80% sand and 7% clay, the poor drainage features of the site resulted in generally wet soil conditions throughout 2007 ($VSM > 24\%$). The ground is flat, and the cover under the tree canopy consists of relatively short grass and weeds that were cut a few times during the year. A gridded metal sheet was inserted into the soil and photographed to estimate surface roughness properties. The photo was corrected for viewing angle variation, and the surface was digitized. From this digital surface, the surface rms height was calculated as 0.5 cm. At the end of October (pre-leaf drop), the relative dielectric constants of the tree constituents were measured at L-band (1.25 GHz) *in situ*, using dielectric probes connected to an HP8719A vector network analyzer. The technique is based on reflection from an open-ended coaxial probe. The measured average relative dielectric constants are $35.2 + i5.3$ for leaves, $12.0 + i2.9$ for branches, and $15.6 + i3.8$ for trunks. To permit proper interpretation of the measured microwave signals, a representative tree outside the microwave footprint was cut down and destructively sampled. Detailed measurements of size/angle distributions of the tree constituents (trunk, branches, and leaves) along with their densities were made. The results from the canopy sampling are shown in Table II. The canopy sampling measurements were used in the time-domain simulations described previously to produce transient responses at the ComRAD incidence angles so that simulation results can be compared with the measured data.

D. Simulation Results and Discussion

In this section, several plots will be presented in order to characterize the backscattering sources of a time-domain radar response. The site description information, summarized in the previous section, has been used to run the Monte Carlo simulations. The behavior of individual responses (direct, direct reflected, and reflected) is considered first. The influence of incidence angle and soil moisture on the transient response of
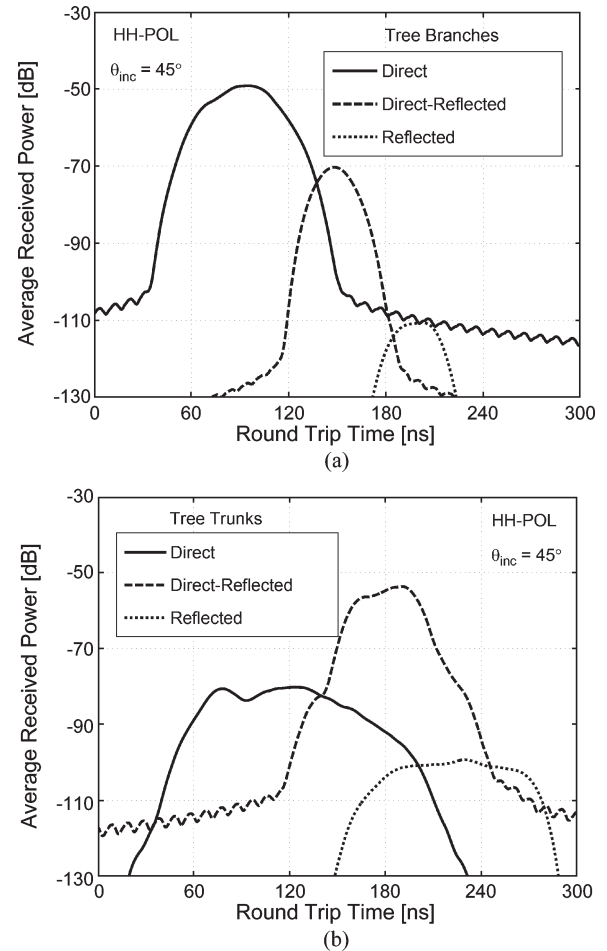

Fig. 4. Individual scattering contributions of HH polarization at the incidence angle of 45°: (a) shows *branch contribution* only. (b) shows *trunk contribution* only.

a forested terrain is then examined through numerical simulations. Finally, the measured backscatter transient responses from Paulownia trees under full-canopy and leaf-drop conditions at 45° are utilized to validate the model for the linear copolarized cases only.

A comparison between the branch and trunk contributions in the transient response at the incidence angle of 45° is shown in Fig. 4(a) and (b), respectively, for HH polarization. Each plot in both figures shows the contribution of the individual scattering components to the overall backscattering transient response. In both plots, the three components of the transient response are distinguishable due to their different arrival times. The direct term arrives first at the antenna. The direct-reflected term is observed later in time due to the relatively longer path it travels, and the reflected term arrives later than the other components since it gets reflected twice from the ground. Fig. 4 shows that the direct backscattering from trunks is relatively small and that the direct term is due mostly to the backscattering from branches. This lower contribution of trunks to the direct term can be attributed to their vertical orientation and low densities. On the other hand, trunks act as a corner reflector; they dominate the direct-reflected component. The contribution of branches to the direct-reflected scattering mechanism is
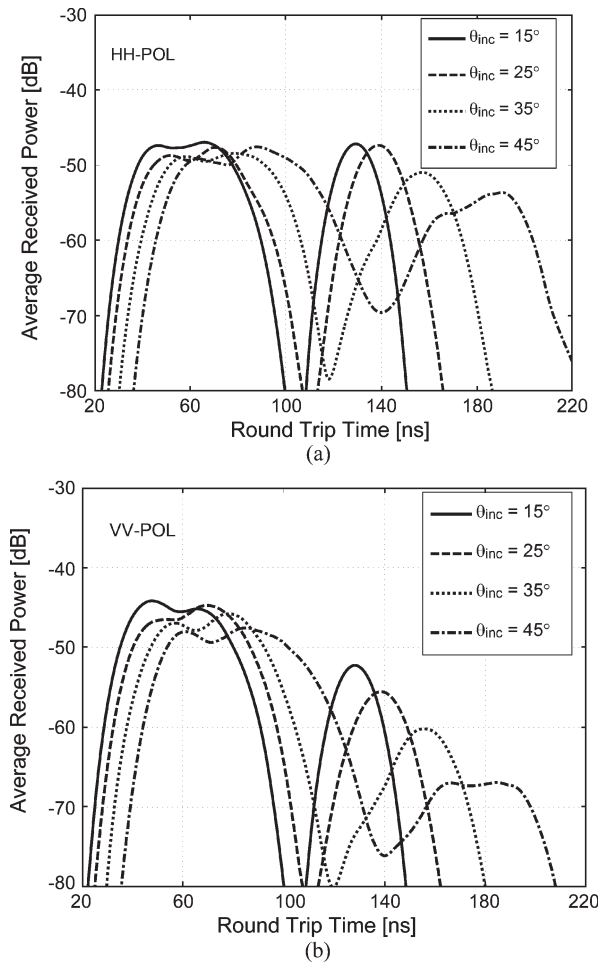
Fig. 5. *Effect of the angle of incidence* on the time-domain radar backscatter response: (a) HH polarization. (b) VV polarization.

somewhat lower. It is clear from the figures that the reflected term is always the smallest and, for most practical cases, can be ignored. It is worth mentioning that the contribution of leaves at L-band to the total backscattering response was found to be negligible compared with the contribution from branches and trunks. The leaves, however, were included in the simulations due to their significant effect on the canopy extinction.

Fig. 5(a) and (b) shows the effects of the incidence angle on the total time-domain responses at the HH and VV polarizations, respectively. It is observed that two peaks dominate the total response. The first peak is due to volume scattering and is sensitive to the structural and dielectric characteristics of forest canopies while the second peak is due to double interaction; its amplitude is proportional to the magnitude of the reflection coefficient from the ground. It is observed that the second peak decreases in magnitude as a function of incidence angle. This decay in the second peak can be explained by noting that the coherent model developed in this paper takes into account the beam divergence inside the vegetation and the variation of the attenuation along the propagation direction. The divergence of beam results in the weaker scattered fields in the bistatic direction since the scattered wave from vertical trunks becomes slightly away from the forward scattering cone [see Fig. 3(b)]. In addition, due to the spread of the incident wave, different

particles in the layer experience different incidence directions. The coherent sum of these scattered waves results in averaging the scattering mechanism strength over the illuminated volume. This effect can also be seen from Fig. 5(a) and (b) that the responses from the medium rise and decay as a smooth function in time [12], [13]. The averaging effect of the beam spread becomes more important at higher angles as a consequence of the fact that the durations of each individual response last longer and overlap with one another with increasing angles. The longer the duration (path length) is, the higher attenuation the wave experiences as well. Thus, the beam divergence and attenuations are less important at low angles, and it appears that, at low incidence angles, double interaction is stronger.

It is also observed that the rate of decrease in the second peak of the VV polarization response is more rapid than that of the HH polarization response. There are several reasons. First, the VV polarization response experiences more attenuation than the HH polarization response does due to the tendency for the branches to be vertically oriented. Second, the ground reflection coefficient of VV polarization drops in magnitude, whereas the magnitude of the ground reflection coefficient of the HH polarization increases slightly with the increase of the incidence angle. As a result, the level of the second peak for the HH polarization becomes considerably larger than the second peak of the VV polarization as the incidence angle increases. This suggests that the interaction term of the HH polarization response acts to enhance the radar sensitivity to the moisture contained in the soil beneath a vegetation canopy as the angle increases. On the other hand, VV polarization is more sensitive to soil moisture variations as observed from the second peak shown in Fig. 6(a) and (b), which shows the effect of soil moisture on the total time-domain responses of the HH and VV polarization radar backscatter, respectively. The solid line in Fig. 6 shows wet (volumetric soil moisture (VSM) of 40%) soil, and the dotted line shows dry (VSM of 5%) soil. It is clear that the first peak remains exactly the same while the second peak varies 3 dB maximum for HH polarization and 6 dB maximum for VV polarization at 45°. The sensitivity of the second peak of the VV polarization response to the soil moisture variations is due mainly to the higher variations of the reflection coefficient of the VV polarization at higher incidence angles.

The comparison between the measured and the simulated transient responses of the HH and VV polarizations at 45° is shown in Fig. 7. The measured VSMs were 24.3% on October 22, 2007 and 32.0% on November 24, 2007. A good agreement is observed between the average simulated and measured backscatter transient responses of the Paulownia trees under the *leaf-drop* (November 24) and the *full-canopy* (October 22) conditions. It is clear from these figures that the components of the transient response arrive at the receiver at different times. Therefore, it is possible to distinguish the characteristics of the forested terrain using L-band stepped-frequency signals as a function of depth. The volume-scattering and double-interaction contributions of the measured data can be separated successfully with the use of temporal bandpass filters in time. Hence, each contribution can be used as a means for obtaining additional information about the layer. For example, the path traveled in the canopy can be used to obtain
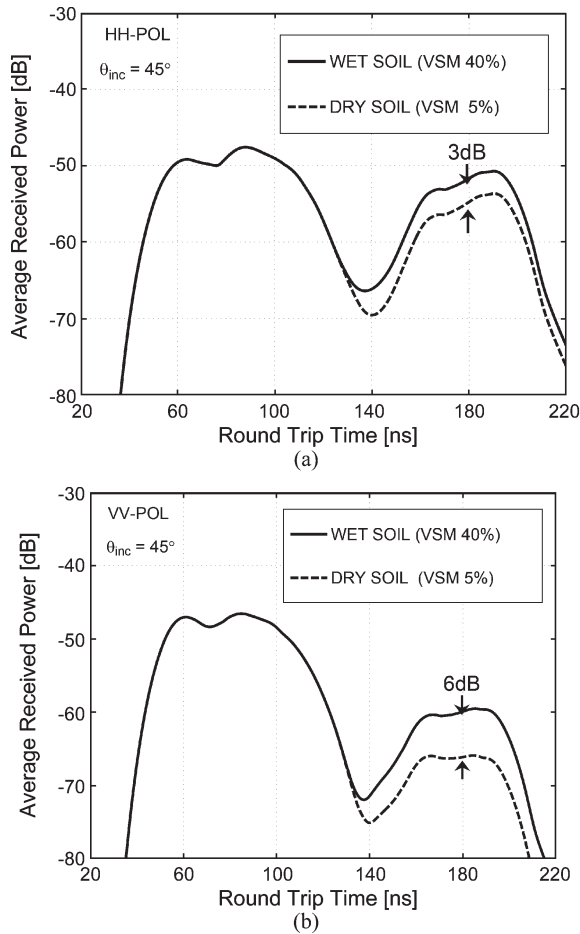
Fig. 6. *Effect of soil moisture* on the time-domain radar backscatter responses at the incidence angle of 45°: (a) HH polarization. (b) VV polarization.

an estimate of the canopy height, and it is clearly evident from the duration of the first peak. It may even be possible to extract the relative height of the crown layer to trunk layer from the time difference between the first- and second-peak returns since these returns are strongly dependent on the layer thickness. Moreover, the second peak, which is a result of canopy–ground interaction, provides information about the dielectric properties of the ground.

III. NEW TECHNIQUE TO ESTIMATE CANOPY ATTENUATION

Rigorous models with many input variables are useful for understanding the sensitivity of the microwave sensor response to a forest canopy. The vegetation transient-response model developed in the previous section is an example of this type of model. We have demonstrated the sensitivity of the time-domain response of individual scattering mechanisms and total radar backscatter to a forest canopy by several parameters such as angle of incidence, soil moisture, and defoliation. On the other hand, simple models that require less parameters and *a priori* information are necessary in the development of reliable inversion algorithms for sensors with a limited number of observations. Therefore, the objective of this section is to develop a simple but physically based algorithm with reduced
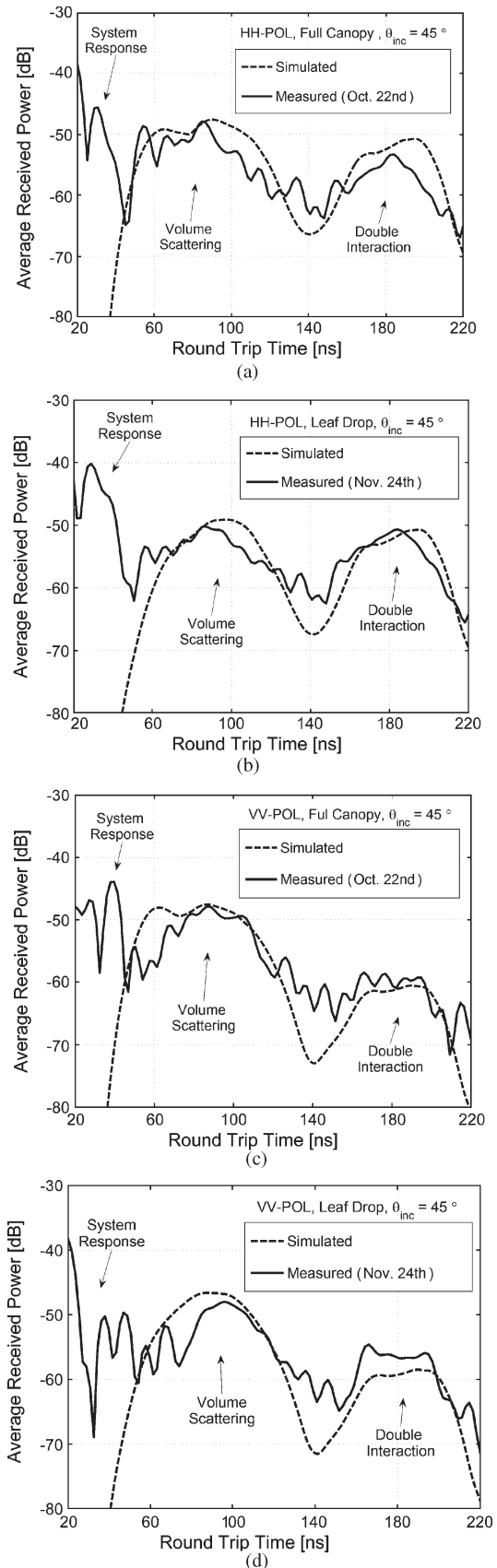

Fig. 7. Comparison between the average measured and simulated backscatter transient responses of Paulownia trees at 45°: (a) shows the *full-canopy* condition for HH polarization. (b) shows the *leaf-drop* condition for HH polarization. (c) shows the *full-canopy* condition for VV polarization. (d) shows the *leaf-drop* condition for VV polarization.

parameterizations for the forest canopy. The algorithm for the estimation of canopy attenuation described here uses radar data to extract vegetation scattering properties. The time-domain information provided by the stepped-frequency measurements at L-band offers a unique opportunity to investigate the scattering behavior of the forest. As shown in the previous section, the forest features that are difficult to observe with conventional σ^0 measurements such as volume scattering from branches and leaves and the double interaction of trunks and branches with the ground can be identified at L-band with a range resolution on the order of a couple of meters in the time-domain response.

The algorithm, presented in this section, is based on separating the canopy and the trunk–ground returns in the radar time-domain backscatter response. One can separate these two contributions by performing a time-gating operation on the measured time-domain response. This involves the following steps: 1) The frequency data are transformed to the time domain; 2) the parameters (time center and span) for the gate filter are identified; 3) a frequency-domain version of the gate is constructed as a zero phase finite-impulse-response filter with a Kaiser–Bessel window; 4) the measured frequency data are extrapolated at each end of the passband since the gating operation on the frequency data distorts the signal level at the frequency edges and generates a ripple at the center frequencies [28]; 5) both the extrapolated frequency-domain data and the gating function after windowing are transformed to the time domain; 6) the time-domain response of the radar backscatter is multiplied by the gate filters whose passband agrees with the volume and the double-interaction responses; 7) the resulting signals are transformed back to the frequency domain; and 8) the corrupted extrapolated data are then discarded, leaving the measured range of frequency data uncorrupted since the distortion mainly affects the extrapolated samples. These steps are summarized in a block diagram in the first half (up to normalization) of the diagram shown in Fig. 9.

Once the individual frequency responses due to the volume-scattering and double-interaction contributions are separated from the data, the FCFs for each backscattering contribution are generated. The backscatter response can be assumed to be a stationary process since the transmitted signal is narrowband, i.e., the bandwidth of the radar is a small fraction of the center frequency (100 MHz/1.25 GHz $\ll 1$). Thus, its covariance can be written as a function of frequency shift Δf. The physical significance of the FCF is that it provides a measure of the magnitude of correlation between target frequency responses at two spaced frequencies. In practice, the FCF from stepped-frequency measurements is computed with the narrowband approximation in the following way [29]:

$$C_{pq}^{\mathrm{msr}}(n\Delta f) = \frac{1}{N_s}\sum_{i=1}^{N_s}\frac{1}{N_f - n}\sum_{j=1}^{N_f - n} E_{pq}^{(i,j)} E_{pq}^{(i,j+n)*},$$

$$\text{for } 0 \leq n \leq N_f - 1 \quad (9)$$

where E^* denotes to complex conjugate of E, the superscript msr stands for the measured quantity, $E_{pq}^{(i,j)}$ denotes the electric field of the ith sample at the jth frequency point, and the
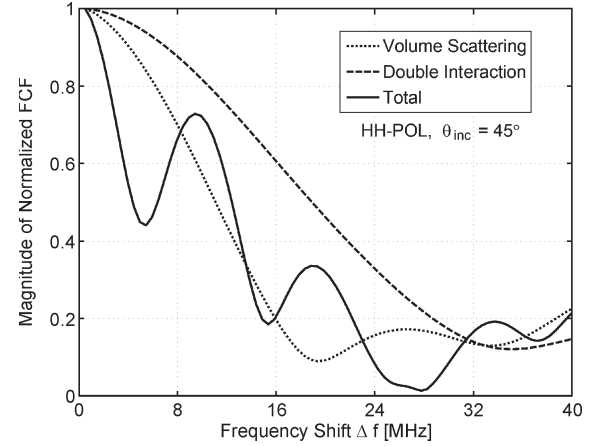

Fig. 8. FCF of the individual scattering mechanisms and overall response of HH polarization at the incidence angle of 45°.

frequency spacing is given by $\Delta f = B/(N_f - 1)$. The statistical averaging is obtained by measuring N_s independent samples. The radar was rotated in a conical scan arrangement in azimuth in order to obtain the statistical averaging needed for the FCF definition given previously. During each scan, 28 independent spatial samples were taken over Paulownia trees.

The decorrelation bandwidth is the range of frequencies over which two frequency components have a strong potential for amplitude correlation. It provides information on the dependence of the target's scattering centers on their relative positions within the medium. In order to characterize the decorrelation behavior of the double-interaction and volume-scattering contributions, the FCF formula given in (9) is applied to data acquired by the ComRAD's radar, which operates in the stepped-frequency mode. The resulting FCF is shown in Fig. 8. As seen from this figure, the FCF of the double-interaction contribution has a larger decorrelation bandwidth than that of the volume scattering. This FCF discrimination between two scattering mechanisms can be explained by noting that the tree trunks (main contributor to the double interaction) are more organized as compared with the branches (main contributor to the volume scattering). In addition, the overall FCF of the radar backscatter response has an oscillatory behavior and very small decorrelation bandwidth due to the constructive and destructive interferences among different scattering mechanisms. This analysis suggests that the FCFs of different scattering mechanisms can be used to infer additional information hidden in their decorrelation behaviors.

An analytical expression for the FCF of the backscatter response from one layer of random medium, composed of particles above a smooth ground surface, was developed by employing a two-frequency version of the DBA [30]. This derivation established a relationship between the complex FCF of the backscatter and the radar and target parameters. It was shown that the effects of the radar parameters can be incorporated into the formulation explicitly, and the FCF can be written in terms of the product of two expressions, one depending only on the radar system parameters and the other one depending only on the vegetation and ground variables. For a received field $E_{qq}(\mathbf{s}, f)$ due to a particle located at $\mathbf{s}$, the FCF is the
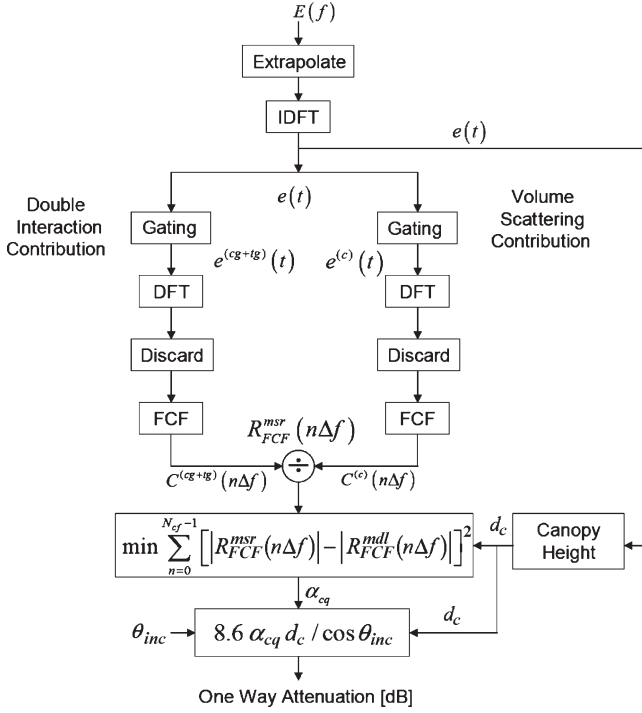
Fig. 9. Data processing scheme.

action terms, respectively; each term is given in Appendix. The reflected and surface scattering terms (after accounting for the extinction of the vegetation) are found to be small and have been omitted from (11).

In (11), the first term is related to the first power peak (volume scattering of the leaves and branches) in the transient solution, whereas the sum of the last two terms is related to the second power peak (the tree–ground interactions). As a result, calculating the ratio of tree–ground to crown-volume returns for the frequency spacing Δf in the passband of the radar results in (12), as shown at the bottom of the page, where the parameter Y_q is equal to $|\Gamma_q|^2 \sigma_{qq\mathrm{dr}}^0 / \sigma_{qqd}^0$, which involves the forest scattering coefficients and the ground reflectance, and the angle θ_{inc} denotes the radar look angle measured from nadir. The quantity σ_{qqd}^0 is the sum of the copolarized backscattering coefficients of leaves (L) and branches (B). The quantity $\sigma_{qq\mathrm{dr}}^0$ is the sum of the copolarized scattering coefficients of leaves (L), branches (B), and trunks (T) in the bistatic direction. There are two advantages to using this normalization given in (12). First, the ratio $R_{\mathrm{FCF}}^{\mathrm{mdl}}(\Delta f)$ becomes independent of the system parameters since the system covariance $C_{qq}^{\mathrm{sys}}(\Delta f)$ cancels out during the normalization process. Therefore, the radar calibration is not necessary. Second, the number of independent parameters to be estimated is reduced with the combined parameter Y_q.

The exponential factor appearing at the end of (12) involves the attenuation in the trunk layer $\exp\{-4\alpha_{tq}\sec\theta_{\mathrm{inc}}d_t\}$ and a phase factor $\exp\{2(i\Delta k\cos\theta_{\mathrm{inc}})d_t\}$, both of which contain the trunk-layer-dependent parameters. The effect of the trunk layer in the total extinction at L-band is relatively small due to the large densities of branches in the crown layer and the small heights of tree trunks [11]. This is typically true for two-layer forest canopies where the trunk layer is composed of vertical trunks. For the deciduous trees considered in this paper, the attenuation in the trunk layer was found about 1 dB. This trunk attenuation factor is assumed to be negligible. Since only the absolute value of the ratio given in (12) will be used in what follows, the phase factor disappears, and the magnitude of the ratio depends only on the canopy thickness d_c, the canopy attenuation coefficient α_{cq}, and a combined parameter Y_q. The number of unknowns can further be reduced by determining the thickness of the crown layer d_c from the vertical projection of the time span of the first backscatter power peak, which corresponds to the path traveled in the canopy.

The calculation of the magnitude of the ratio given in (12) for an array of frequency spacings over the system bandpass provides a system of equations. To solve for the parameters such as the attenuation α_{cq} and the combined parameter Y_q, a multidimensional unconstrained nonlinear minimization

cross-correlation integral of this field with itself, at a frequency shift Δf, and is given by

$$C_{qq}^{\mathrm{mdl}}(\Delta f) = \int_V d\mathbf{s}\, \langle E_{qq}(\mathbf{s}, f) E_{qq}^*(\mathbf{s}, f + \Delta f)\rangle$$
$$= C_{qq}^{\mathrm{sys}}(\Delta f) C_{qq}^{\mathrm{veg}}(\Delta f) \tag{10}$$

where the superscripts mdl, sys, and veg stand for model, system, and vegetation, respectively. The integral in (10) is taken over the illuminated volume V. The angle bracket denotes ensemble average. The system covariance is denoted by the $C_{qq}^{\mathrm{sys}}(\Delta f)$, and it depends on incidence angle, frequency, polarization, and the height of the antenna. The $C_{qq}^{\mathrm{veg}}(\Delta f)$ denotes the covariance function of vegetation. Here, q is the polarization of the incident, as well as the received wave. The quantity q can be horizontal (H) or vertical (V). Only the copolarized case for FCF is considered in the present investigation.

The $C_{qq}^{\mathrm{veg}}(\Delta f)$ for a two-layer forest canopy over a rough ground surface is composed of three dominant terms, i.e.,

$$C_{qq}^{\mathrm{veg}}(\Delta f) = C_{qq}^{(c)}(\Delta f) + C_{qq}^{(cg)}(\Delta f) + C_{qq}^{(tg)}(\Delta f) \tag{11}$$

where the superscripts c, cg, and tg denote the crown volume scattering, crown–ground interaction, and trunk–ground inter-

$$R_{\mathrm{FCF}}^{\mathrm{mdl}}(\Delta f) = \frac{C_{qq}^{(cg)}(\Delta f) + C_{qq}^{(tg)}(\Delta f)}{C_{qq}^{(c)}(\Delta f)}$$

$$= \frac{[2(i\Delta k\cos\theta_{\mathrm{inc}} - 2\alpha_{cq}\sec\theta_{\mathrm{inc}})d_c]\, e^{2(i\Delta k\cos\theta_{\mathrm{inc}} - 2\alpha_{cq}\sec\theta_{\mathrm{inc}})d_c}}{\left(1 - e^{2(i\Delta k\cos\theta_{\mathrm{inc}} - 2\alpha_{cq}\sec\theta_{\mathrm{inc}})d_c}\right)} Y_q e^{2(i\Delta k\cos\theta_{\mathrm{inc}} - 2\alpha_{tq}\sec\theta_{\mathrm{inc}})d_t} \tag{12}$$

TABLE III
ESTIMATED ONE-WAY ATTENUATION (IN DECIBELS) VALUES FROM
MEASURED DATA AT MULTIPLE INCIDENCE ANGLES AND UNDER
FULL-CANOPY AND LEAF-DROP CONDITIONS

	Full Canopy		Leaf Drop	
Angle	*h-pol*	*v-pol*	*h-pol*	*v-pol*
15^0	6.4	7.1	6.0	6.5
25^0	7.9	8.5	7.1	7.1
35^0	8.9	8.7	8.0	8.1
45^0	10.6	12.3	9.6	12.0

algorithm (MATLAB's *fminsearch* function) is employed. The procedure is based on minimizing the merit function

$$\min \sum_{n=0}^{N_{cf}-1} \left[\left| R_{\text{FCF}}^{\text{msr}}(n\Delta f) \right| - \left| R_{\text{FCF}}^{\text{mdl}}(n\Delta f) \right| \right]^2,$$
$$\text{for } 0 \leq n \leq N_{cf} - 1 \quad (13)$$

where α_{cq} and Y_q act as free parameters and N_{cf} is the number of samples in the decorrelation bandwidth. Once the canopy attenuation coefficient is estimated by minimizing (13), the one-way attenuation in decibels through the canopy can be calculated using the following relationship:

$$One\text{-}Way\ Attenuation \text{ (in decibels)} = -10 \log \gamma_q \quad (14)$$

where the transmissivity γ_q of the canopy is related to the attenuation coefficient α_{cq} of the tree canopy by $\gamma_q = \exp(-2\alpha_{cq}d_c/\cos\theta_{\text{inc}})$. The overall procedure of the proposed technique for determining the attenuation from the measured backscatter response is summarized in a block diagram shown in Fig. 9.

To evaluate the performance of the technique against physical conditions and incidence-angle variations, it is applied to the measured data acquired over the Paulownia trees for the *leaf-drop* and the *full-canopy* conditions at the multiple incidence angles. The resultant estimated attenuation values are shown in Table III. A quick look at the attenuation table shows that lower attenuation values are obtained for the defoliated canopy than those obtained for the foliated canopy for both polarizations. It is also apparent from the table that, as the incidence angle increases from 15° to 45°, the attenuation values increase due to the increase in the path length for the waves to travel within vegetation. At higher angles of incidence, the rate of increase in the attenuation values for VV polarization is observed to be higher than that for HH polarization due to the vertically oriented structure of the trees. At lower incidence angles, however, both the HH and VV polarizations experience similar attenuations. As a result, the technique is shown to be able to sense changes in physical conditions successfully. The results obtained here at 45° are similar to the results at 40° reported by Ulaby *et al.* [31]; they used a completely different approach but a similar instrument configuration. On the other hand, it should be noted that these algorithms have been applied to the truck-based systems, where the antenna is located close to the forest canopy, and as a result, the beam divergence and spreading loss are important and may cause

an overestimation of the attenuation values. These effects are negligible for the pencil beam or SAR airborne radar systems. The adaptation of the technique to these geometries is currently underway.

IV. CONCLUSION

A mathematical formulation characterizing the time-domain radar backscatter response of a distributed medium over a rough surface such as a forested terrain has been developed. The transient response due to the plane-wave spectral components that are excited by the antenna was found. The results were then used to develop a procedure for simulating the time-domain radar backscatter response. Using this procedure, a time-domain analysis for various cases was carried out in order to understand the backscattering sources within a forest canopy and their effects on the transient response. The vegetation transient-response model for linear copolarized cases has been validated with data collected over Paulownia trees under full-canopy and leaf-drop conditions at 45°. It has been shown that it is possible to distinguish the characteristics of the forested canopy as a function of depth by utilizing the different arrival times of the components of the transient response. A time-domain analysis of the radar backscatter response provides an insight into the problem of scattering from forests in time. For example, the time difference between volume-scattering and double-interaction peaks can provide the relative height of the crown to trunk layer. The double-interaction term can be used to estimate soil moisture after crown attenuation is corrected for. Hence, each contribution can be used as a means for obtaining additional information about the layer.

Combining active/passive sensors for the remote sensing of soil moisture through forest canopies provides complementary information contained in the emissivity and backscatter signatures. While passive sensors are more sensitive to soil moisture and are more stable relative to small changes in surface and vegetation parameters, active sensors have a better sensitivity to forest structures with higher resolution. For the radiometric remote sensing of soil moisture, the presence of trees causes attenuation to the soil emission underneath. The correction for the vegetation effects, which is required in passive algorithms, can be accomplished by utilizing backscatter signals. For this purpose, a new technique for determining the canopy attenuation using the measured stepped-frequency radar backscatter response has been proposed in this paper. The technique is applicable when the forest height is sufficient to separate individual scattering mechanisms in the radar backscatter transient response. The algorithm normalizes the FCF of the direct-reflected term to the FCF of the direct term, which are calculated after the separation of these contributions in time domain. It has been shown that the magnitude of this ratio is independent from radar parameters and is a function of the attenuation coefficient, canopy thickness, and a combined parameter that involves surface reflectance and canopy scattering coefficients. The technique was applied to the ComRAD stepped-frequency radar data collected over stands of deciduous Paulownia trees under various physical conditions; canopy attenuation was successfully retrieved.

Our results suggest that further exploitation of radar data in time–frequency domains leads to a physically based algorithm that requires less parameters and *a priori* information. This is a desirable step toward better benefiting from spaceborne microwave sensors that have a limited number of observations. Our current research is directed toward adapting this technique to current and future L-band active sensors with a scanning pencil-beam instrument or fine-resolution SAR. Having the forest attenuation information on a global basis will help to extend accurate soil moisture retrievals from global microwave missions to more areas of the Earth's surface than are currently feasible.

APPENDIX
COPOLARIZATION FCF FOR A TWO-LAYER FOREST CANOPY

The DBA is used to obtain the FCF for a forest canopy consisting of two layers of vegetation over a rough ground surface. The scattered fields are computed by employing the single-scattering theory such that the incident and scattered waves propagate with the characteristics of the mean wave. The backscattered fields are then correlated at two different frequencies separated by a frequency shift Δf. The resulting FCF has its maximum magnitude at zero frequency shift ($\Delta f = 0$), which is also equivalent to the backscattering coefficients of the medium. Then, the FCF decreases in magnitude but not monotonically as the frequency shift increases due to the change of the relative phase angle of the signal with frequency.

Using the single-scattering theory [19], [20], the dominant terms of the forest covariance function appearing in (11) of Section III can be expressed in terms of scattering cross sections, wave attenuation, and reflection properties of the ground as follows:

1) *Crown Volume Scattering:*

$$C_{qq}^{(c)}(\Delta f) = \left[\rho_L \sigma_{qqd}^{(L)} + \rho_B \sigma_{qqd}^{(B)}\right] \left(\frac{1 - e^{-2\chi_{cq} d_c}}{2\chi_{cq}}\right) \quad \text{(A1a)}$$

2) *Crown–Ground Double Interaction:*

$$C_{qq}^{(cg)}(\Delta f) = \left[\rho_L \sigma_{qq\mathrm{dr}}^{(L)} + \rho_B \sigma_{qq\mathrm{dr}}^{(B)}\right] |\Gamma_{gq}|^2 d_c e^{-2(\chi_{cq} d_c + \chi_{tq} d_t)} \quad \text{(A1b)}$$

3) *Trunk–Ground Double Interaction:*

$$C_{qq}^{(tg)}(\Delta f) = \rho_T \sigma_{qq\mathrm{dr}}^{(T)} |\Gamma_{gq}|^2 d_t e^{-2(\chi_{cq} d_c + \chi_{tq} d_t)} \quad \text{(A1c)}$$

where the thicknesses for the trunk and crown layers are given by d_t and d_c, respectively, and the superscripts L, B, and T refer to leaves, branches, and trunks, respectively. The corresponding number of scatterers per unit volume are given by ρ_L, ρ_B, and ρ_T, respectively. The quantities $\sigma_{qqd}^{(\alpha)}$ and $\sigma_{qq\mathrm{dr}}^{(\alpha)}$ represent scattering cross sections of type $\alpha \in \{L, B, T\}$ in backscattering (denoted by the subscript d) and bistatic (denoted by the subscript dr) directions, respectively. Here, the interface between vegetation and ground is taken to be rough; thus, the crown–ground and trunk–ground interactions involve the reflectivity of the rough surface which is described in (7) of Section II.

The χ_{cq} and χ_{tq} appearing in the aforementioned expressions are related to the frequency shift and the canopy attenuation coefficients of crown α_{cq} and trunk α_{tq} layers, respectively, and they are given as follows:

$$\chi_{cq} = 2\alpha_{cq} \sec \theta_{inc} - i\Delta k \cos \theta_{inc}$$
$$\alpha_{cq} = \frac{2\pi}{k_0} \Im m \left\{\rho_L \overline{f_{qq}^{(L)}}(\hat{\mathbf{i}}, \hat{\mathbf{i}}) + \rho_B \overline{f_{qq}^{(B)}}(\hat{\mathbf{i}}, \hat{\mathbf{i}})\right\} \quad \text{(A2a)}$$
$$\chi_{tq} = 2\alpha_{tq} \sec \theta_{\text{inc}} - i\Delta k \cos \theta_{\text{inc}}$$
$$\alpha_{tq} = \frac{2\pi}{k_0} \Im m \left\{\rho_T \overline{f_{qq}^{(T)}}(\hat{\mathbf{i}}, \hat{\mathbf{i}})\right\} \quad \text{(A2b)}$$

where the subscripts c and t denote the crown and trunk layers, respectively, k_0 is the free space wavenumber, $\Delta k = 2\pi\Delta f/c$, and c is the speed of light. The bar over the scattering amplitudes denotes ensemble average over the angular and size statistics of particles. The quantity $f_{qq}^{(\alpha)}(\hat{\mathbf{i}}, \hat{\mathbf{i}})$ is the copolarized forward scattering amplitude of scatter type $\alpha \in \{L, B, T\}$, and the unit vector $\hat{\mathbf{i}}$ represents the direction of propagation. The real part of the propagation constant is dominated by the free-space component since the fractional volume occupied by the vegetation is small. The effect of the imaginary part (specific attenuation), however, can be appreciable.

REFERENCES

[1] H. M. J. Barre, B. Duesmann, and Y. H. Kerr, "SMOS: The mission and the system," *IEEE Trans. Geosci. Remote Sens.*, vol. 46, no. 3, pp. 587–593, Mar. 2008.

[2] "Earth science and applications from space: National imperatives for the next decade and beyond," Nat. Res. Council, Washington DC, Jan. 2007. Tech. Rep.

[3] G. Macelloni, S. Palocia, P. Pampolaloni, and R. Ruisi, "Airborne multi-frequency L- and Ka-band radiometric measurements over forests," *IEEE Trans. Geosci. Remote Sens.*, vol. 39, no. 11, pp. 2507–2513, Nov. 2001.

[4] P. Ferrazolli, L. Guerriero, and J. P. Wigneron, "Simulating L-band emission of forests in view of future satellite applications," *IEEE Trans. Geosci. Remote Sens.*, vol. 40, no. 12, pp. 2700–2708, Dec. 2002.

[5] S. S. Saatchi, K. Halligan, D. G. Despain, and R. L. Crabtree, "Estimation of forest fuel load from radar remote sensing," *IEEE Trans. Geosci. Remote Sens.*, vol. 45, no. 6, pp. 1726–1740, Jun. 2007.

[6] L. Thirion-Lefvre and E. Colin-Koeniguer, "Investigating attenuation, scattering phase center, and total height using simulated interferometric SAR images of forested areas," *IEEE Trans. Geosci. Remote Sens.*, vol. 45, no. 10, pp. 3172–3179, Oct. 2007.

[7] A. Rosenqvist, M. Shimada, N. Ito, and M. Watanabe, "ALOS PALSAR: A pathfinder mission for global-scale monitoring of the environment," *IEEE Trans. Geosci. Remote Sens.*, vol. 45, no. 11, pp. 3307–3316, Nov. 2007.

[8] M. C. Dobson, F. T. Ulaby, L. Pierce, T. L. Sharik, K. M. Bergen, J. M. Kellndorfer, J. R. Kendra, E. Li, Y. C. Lin, A. Nashashibi, K. Sarabandi, and P. Siqueira, "Estimation of forest biophysical characteristics in Northern Michigan with SIR-C/X-SAR," *IEEE Trans. Geosci. Remote Sens.*, vol. 33, no. 4, pp. 877–895, Jul. 1995.

[9] S. S. Saatchi and M. Moghaddam, "Estimation of crown and stem water content and biomass of boreal forest using polarimetric SAR imagery," *IEEE Trans. Geosci. Remote Sens.*, vol. 38, no. 2, pp. 697–709, Mar. 2000.

[10] K. P. Papathanassion, S. R. Cloude, A. Reiber, and W. M. Boerner, "Multibaseline polarimetric SAR interferometry for vegetation parameter estimation," in *Proc. Int. Geosci. Remote Sens. Symp.*, Honolulu, HI, Jul. 2000, pp. 2762–2764.

[11] S. S. Saatchi and K. C. McDonald, "Coherent effects in microwave backscattering models for forest canopies," *IEEE Trans. Geosci. Remote Sens.*, vol. 35, no. 4, pp. 1032–1044, Jul. 1997.

[12] D. Le Vine, R. H. Lang, and Y. Lin, "Transient response of a layer of discrete random media over a dielectric half space," *IEEE Trans. Geosci. Remote Sens.*, vol. 30, no. 5, pp. 1034–1045, Sep. 1992.

[13] O. Kilic and R. H. Lang, "Scattering of a pulsed beam by a random medium over ground," *J. Electromagn. Waves Appl.*, vol. 15, no. 4, pp. 481–516, 2001.

[14] R. Zoughi, L. K. Wu, and R. K. Moore, "Identification of major backscattering sources in trees and shrubs at 10 GHz," *Remote Sens. Environ.*, vol. 19, no. 3, pp. 269–290, Jun. 1986.

[15] J. Hyyppa and M. T. Hallikainen, "A helicopter-borne eight-channel ranging scatterometer for remote sensing: Part 2: Forest inventory," *IEEE Trans. Geosci. Remote Sens.*, vol. 31, no. 1, pp. 170–179, Jan. 1993.

[16] J. M. Martinez, N. Floury, T. Le Toan, A. Beaudoin, M. T. Hallikainen, and M. Makynen, "Measurements and modeling of vertical backscatter distribution in forest canopy," *IEEE Trans. Geosci. Remote Sens.*, vol. 38, no. 2, pp. 710–719, Mar. 2000.

[17] R. H. Lang, R. Landry, O. Kavaklioglu, and J. C. Deguise, "Simulation of microwave backscatter from a red pine stand," in *Proc. SPIE, Multispectral Microw. Sens. Forestry, Hydrol. Natural Resources*, Rome, Italy, 1994, vol. 2314, pp. 538–548.

[18] N. M. Khadr, "Wave correlation effects in active microwave remote sensing of the environment," Ph.D. dissertation, George Washington Univ., Washington DC, 1994.

[19] R. H. Lang, "Electromagnetic backscattering from a sparse distribution of lossy dielectric scatterers," *Radio Sci.*, vol. 16, no. 1, pp. 15–30, Jan./Feb. 1981.

[20] R. H. Lang and J. Sidhu, "Electromagnetic backscattering from a layer of vegetation: A discrete approach," *IEEE Trans. Geosci. Remote Sens.*, vol. GRS-21, no. 1, pp. 62–71, Jan. 1983.

[21] W. Wasylkiwskyj and J. Alatishe, "Coherent scattering from distributed targets," in *Proc. IEEE Microw., Radar, Remote Sens. Symp.*, Kiev, Ukraine, Sep. 2008, pp. 36–41.

[22] L. Tsang, J. A. Kong, and R. Shin, *Theory of Microwave Remote Sensing*. New York: Wiley-Interscience, 1985.

[23] *E5071B ENA Series Vector Network Analyzer Operating Manual*, Hewlett Packard, Santa Rosa, CA, 2001.

[24] B. D. Jersak, M. Dolaty, and A. J. Blanchard, "Time domain enhancement of frequency domain radar cross-section data," *Int. J. Remote Sens.*, vol. 13, no. 11, pp. 2105–2119, 1992.

[25] P. E. O'Neill, R. H. Lang, M. Kurum, K. R. Carver, and C. Utku, "Multisensor microwave remote sensing of NASA's combined radar/radiometer (ComRAD) system," in *Proc. MicroRad*, San Juan, Puerto Rico, Feb. 2006, pp. 50–54.

[26] P. E. O'Neill, R. H. Lang, M. Kurum, A. T. Joseph, T. J. Jackson, M. H. Cosh, and R. Nelson, "ComRAD active/passive microwave measurements of tree canopies," in *Proc. Int. Geosci. Remote Sens. Symp.*, Barcelona, Spain, Jul. 2007, pp. 1420–1423.

[27] R. Nelson, G. Parker, and M. Hom, "A portable airborne laser system for forest inventory," *Photogramm. Eng. Remote Sens.*, vol. 49, no. 3, pp. 267–273, 2003.

[28] R. P. Yague, A. B. Ibars, and L. F. Martinez, "Analysis and reduction of distortions induced by time-domain filtering techniques in network analyzers," *IEEE Trans. Instrum. Meas.*, vol. 47, no. 4, pp. 930–934, Aug. 1998.

[29] A. A. Monakov, J. Vivekanandan, A. S. Stjernman, and A. K. Nystrom, "Spatial and frequency averaging techniques for a polarimetric scatterometer system," *IEEE Trans. Antennas Propag.*, vol. 32, no. 1, pp. 187–196, Jan. 1994.

[30] K. Sarabandi and A. Nashashibi, "Analysis and application of backscattered frequency correlation function," *IEEE Trans. Geosci. Remote Sens.*, vol. 37, no. 4, pp. 1895–1906, Jul. 1999.

[31] F. T. Ulaby, M. W. Whitt, and M. C. Dobson, "Measuring the propagation properties of a forest canopy using a polarimetric scatterometer," *IEEE Trans. Antennas Propag.*, vol. 38, no. 2, pp. 251–258, Feb. 1990.

Roger H. Lang (F'89) received the B.S. and M.S. degrees in electrical engineering and the Ph.D. degree in electrophysics from the Polytechnic University, New York, NY, in 1962, 1964, and 1968, respectively.

From 1963 to 1964, he was with Bell Telephone Laboratories, where he worked on satellite antennas. From 1968 to 1970, he was with the Courant Institute of Mathematical Science, New York University, where he has done postdoctoral work on wave propagation in random media. He is currently the T. Stanley Crane Professor of engineering and applied science with the Department of Electrical and Computer Engineering, The George Washington University, Washington, DC. He is a member of the editorial board of *Waves in Random and Complex Media*.

Dr. Lang is the Chairman of the U.S. National Committee/International Union of Radio Science Commission F.

Peggy E. O'Neill (M'85–SM'03) received the B.S. (*summa cum laude*, with university honors) degree in geography from Northern Illinois University, DeKalb, in 1976 and the M.A. degree in geography from the University of California, Santa Barbara, in 1979.

She also spent a year with Cornell University, Ithaca, NY, where she did postgraduate work in civil and environmental engineering. Since 1980, she has been a Physical Scientist with the Hydrological Sciences Branch, Hydrospheric and Biospheric Sciences Laboratory, National Aeronautics and Space Administration (NASA) Goddard Space Flight Center, Greenbelt, MD, where she conducts research in soil moisture retrieval and land-surface hydrology, primarily through microwave remote sensing techniques. She is the Deputy Project Scientist for NASA's Soil Moisture Active and Passive soil moisture mission.

Mehmet Kurum received the B.S. degree in electrical and electronics engineering from Boğaziçi University, Istanbul, Turkey, in 2003 and the M.S. degree in electrical engineering from The George Washington University (GWU), Washington, DC, in 2005, where he is currently working toward the Ph.D. degree with a research topic in "Soil Moisture Retrieval Development with a Combined Radar/Radiometer (ComRAD) System" in the Department of Electrical and Computer Engineering.

Since 2003, he has been a Research Assistant with GWU, where he conducts research in the microwave remote sensing of soil moisture retrieval through a forest canopy, the development of the National Aeronautics and Space Administration (NASA)'s ComRAD system, the design of network-analyzer-based radar for NASA's 2-km microwave link, and the development of algorithms to measure rainfall over the link.

Alicia T. Joseph received the B.S. degree in environmental science from Medgar Evers College, City University of New York, Brooklyn, in 1998, the M.S. degree in environmental and occupational health science from Hunter College, City University of New York, New York, in 2000, and the M.S. degree in geography and environmental engineering from The Johns Hopkins University, Baltimore, MD, in 2004. She is currently working toward the Ph.D. degree with a research topic in "Physical and Semi-Empirical Approaches to Quantifying Microwave Optical Depth of Vegetation to Improve Estimates of Soil Moisture" at the University of Maryland, College Park.

Since 2001, she has been with the Hydrological Sciences Branch, Hydrospheric and Biospheric Sciences Laboratory, National Aeronautics and Space Administration Goddard Space Flight Center, Greenbelt, MD, where she conducts research in the microwave remote sensing of soil moisture retrieval.

Thomas J. Jackson (A'86–M'96–F'02) received the Ph.D. degree from the University of Maryland, College Park, in 1976.

He has been with the Hydrology and Remote Sensing Laboratory, U.S. Department of Agriculture Agricultural Research Service, Beltsville, MD, since 1977, where he is currently a Research Hydrologist. He is or has been a member of the science and validation teams of the Aqua, Advanced Earth Observing Satellite-II, Radarsat, Oceansat-1, Envisat, Advanced Land Observing Satellite, and the Soil Moisture and Ocean Salinity remote sensing satellite. His research involves the application and development of remote sensing technology in hydrology and agriculture, primarily in the microwave measurement of soil moisture.

Dr. Jackson is a Fellow of the American Meteorological Society and the American Geophysical Union. He is a member of the IEEE Geoscience and Remote Sensing Administrative Committee, where he serves as Secretary. In 2003, he was the recipient of the AGU Hydrology Award and the William T. Pecora Award (National Aeronautics and Space Administration and Department of Interior) for his outstanding contributions toward understanding the Earth by means of remote sensing.

Michael H. Cosh received the B.A. degree in engineering, with minors in math and physics, from Saint Francis College, Loretto, PA, in 1995, the B.S. degree (*magna cum laude*, with honors) in civil and environmental engineering from The Pennsylvania State University, University Park, in 1996, and the M.S. degree in hydraulics and hydrology and the Ph.D. degree in environmental fluid mechanics and hydrology from the School of Civil and Environmental Engineering, Cornell University, Ithaca, NY, in 1998 and 2002, respectively.

He is currently with the Hydrology and Remote Sensing Laboratory, U.S. Department of Agriculture Agricultural Research Service, Beltsville, MD. His research interest lies in *in situ* soil moisture network validation, scaling of land-surface parameters to satellite scale, and leaf wetness characterization and its interaction with microwave remote sensing.